

Influences of Basicity and Li₂O on the Properties of Fluorine-Free Mold Flux for the Casting of Medium Carbon Steels



WANLIN WANG, XIONG YAN, LEJUN ZHOU, SENLIN XIE, and DAOYUAN HUANG

An investigation was carried out to study the influences of basicity and Li₂O on the melting, crystallization, and heat transfer behavior of Fluorine-free mold flux designed for the casting of medium carbon steels using double hot thermocouple technology and infrared emitter technique. The results showed that with the addition of basicity, the melting and crystallization temperatures of the mold fluxes were increased, and the final heat transfer rate was reduced, as the basicity tends to promote the crystallization behavior of the designed mold fluxes. Besides, with the increase of Li₂O content in the mold flux, the melting and crystallization temperature decreased, as the Li₂O tends to inhibit the formation of high melting temperature crystal and lower the system melting temperature zone; meanwhile the crystallization capability of the mold flux was enhanced in the low-temperature region. Moreover, the results of EDS and XRD were confirmed that the main crystal phase in the Fluorine-free mold fluxes is calcium borate silicate (Ca₁₁Si₄B₂O₂₂). Those results obtained can provide guidelines for the design of new Fluorine-free mold flux for the casting medium carbon steels.

DOI: 10.1007/s11663-016-0597-x

© The Minerals, Metals & Materials Society and ASM International 2016

I. INTRODUCTION

IT is well known that mold fluxes play important roles in continuous casting, such as protecting the molten steel from oxidation, absorbing inclusions, providing the thermal insulation, lubricating the strand, and controlling the heat transfer between the mold and steel shell.^[1] Generally the commercial mold fluxes contain 5 to 10 pct CaF₂ which tends to control the viscosity and melting temperature of the mold flux,^[2,3] as the fluoride can reduce the polymerization of the silicate network and the viscosity of silicate slag.^[4]

Although fluorides play important roles in the mold flux system, *i.e.*, reducing viscosity and break temperature to improve lubrication ability and forming cuspidine (Ca₄Si₂O₇F₂) to control the heat flux in the mold;^[5] however, it would be evaporated and released to the environment in the form of HF, SiF₄, NaF, *etc.*, during the process of casting. Thus, these fluorides will lead to the corrosion of equipment, serious environmental pollution, *etc.*^[6,7] Therefore the development of new environmental friendly F-free mold fluxes is of great importance.

As it is well known, longitudinal cracks may form on the slab surface when casting medium carbon (MC) steels, which is mainly caused by the volumetric

shrinkage during δ - γ phase transformation. Therefore, the heat transfer across the mold flux during the casting of MC steels must be reduced and keep uniform to minimize the thermal stress induced by the volumetric shrinkage. Consequently, the crystallization of the mold flux is very important, and the main challenge of developing F-free mold flux for casting medium carbon steels is to obtain a suitable crystalline phase to replace cuspidine, such that the heat transfer could be effectively controlled to solve above longitudinal cracks.

Nakada *et al.*^[3,7,8] studied the crystallization behaviors of CaO-SiO₂-TiO₂ slag system and their results suggested that the precipitate CaO·SiO₂·TiO₂ in the F-free mold flux could be a substitute for cuspidine. However, Wang *et al.* found that the formation of the high melting point compounds such as TiN and Ti(C,N) in the liquid slag during the casting process may cause the increase of viscosity, break temperature, T_{br} and crystallization temperature, which leads to a lack of lubrication and the tendency of sticker breakout.^[9] In other words, TiO₂ may not be an ideal substitute for fluoride in the F-free mold fluxes.

Recent studies of Wang^[10] indicated that Ca₁₁Si₄B₂O₂₂ precipitated in the low fluorine mold fluxes shows an ideal potential for the substitution of cuspidine. But the crystallization property of the designed F-free mold flux is not strong enough compared with the benchmark flux sample. Previous studies^[11,12] suggested that the crystallization of mold flux could be enhanced by the addition of certain amount of Li₂O and the improvement of basicity (R), which is usually defined as the mass ratio of CaO to SiO₂.^[13]

However, very few studies about the effects of Li₂O and basicity on the heat transfer, melting, and crystallization properties of fluorine-free mold flux have been

WANLIN WANG, Shenghua Professor, XIONG YAN and SENLIN XIE, Graduate Students, and LEJUN ZHOU and DAOYUAN HUANG, Lecturers, are with the School of Metallurgy and Environment, Central South University, Changsha 410083, P.R. China. Contact e-mails: wanlin.wang@gmail.com; l.j.zhou@hotmail.com

Manuscript submitted August 4, 2015

Article published online February 1, 2016.

conducted for the casting of MC steels due to the difficulty of the controlling of the crystallization and heat transfer behavior without the formation of cuspidine. Also the influence of Li_2O and basicity on those properties of F-free mold fluxes has not been thoroughly understood. Therefore, it is essential to conduct above study systematically for the better design of F-free mold flux system for the casting of MC steels.

II. EXPERIMENTAL APPARATUS AND METHOD

A. Sample Preparation

The major chemical composition of the testing samples are listed in Table I, where Sample 1 (S1) is a typical industrial F-containing mold flux for the casting of MC steels as the benchmark slag,^[10] while Samples 2, 3, and 4 (S2, S3, S4) are the designed F-free mold fluxes with varied basicity (R) of 1.15, 1.2, and 1.25 and a constant concentration of Li_2O . Samples 2, 5, and 6 (S2, S5, S6) that with a constant basicity of 1.15 are varied with Li_2O content of 2, 4, and 6 pct, respectively. All of these samples are prepared with pure chemical reagents of CaCO_3 , SiO_2 , CaF_2 , B_2O_3 , Al_2O_3 , and Li_2CO_3 etc.

The preparation for the mold flux disks and powders are as follows: first, all the chemical reagents were fully mechanically mixed, and then they were pre-melted at 1773 K (1500 °C) in a graphite crucible for 10 minutes to homogenize its chemical composition. The melting slag was then quenched from its molten state onto a stainless steel plate at room temperature to achieve a glass phase disk. Then the mold flux disk was polished with the sand papers to control its surface roughness and thickness (4.4 mm). In addition, some excess melting slag was quenched by water, then dried, and grounded into powders for double hot thermocouple technology (DHTT) and melting tests.

B. Hot Thermocouple (HTT) Tests

The illustration of hot thermocouple experimental setup is shown in Figure 1; detailed information has been illustrated in the previous study.^[14] In this paper, single hot thermocouple technique (SHTT) was used to conduct the melting and continuous cooling test (CCT), as well as the time–temperature transformation (TTT) tests. The double hot thermocouple technique (DHTT) was adopted to study the mold flux crystallization behavior under the simulated temperature field between the copper mold and initial solidified shell.^[1]

For the melting and CCT tests, the thermal profile is shown in Figure 2(a), where the sample powders were adhered on a B-type thermocouple and then heated from room temperature to 1773 K (1500 °C) at a rate of 15 K/second. Simultaneously, the melting temperature could be obtained during the heating period. Then the molten sample was continuously cooled at a certain cooling rate after it was held for 5 minutes at 1773 K (1500 °C) to homogenize its chemical composition and eliminate bubbles in the molten slag.^[10] For TTT tests, in Figure 2(b), it is the same as CCT tests in the heating and holding period, then the molten sample was quenched to different target temperatures for isothermal crystallization. Unlike CCT tests, the thermal profile for crystallization simulation tests (DHTT tests) was set in a certain temperature field as shown in Figure 2(c). Firstly the two B-type thermocouples were heated from room temperature to 1773 K and 1673 K (1500 °C and 1400 °C) respectively at a rate of 15 K/second. Then the left thermocouple (CH-1) was held at 1773 K (1500 °C) constantly, and the right thermocouple (CH-2) was first held at 1673 K (1400 °C) for 1 minute and then cooled to 1073 K (800 °C) at the cooling rate of 30 K/second. Then the final mold flux film structure will be developed in this temperature gradient to simulate the one occurred in the caster as suggested by Lu.^[1] The experimental phenomenon was recorded by a digital camera, which was connected through a high-temperature microscope.

C. Heat Transfer Tests

The heat transfer tests were conducted through infrared emitter technique (IET) and the schematic

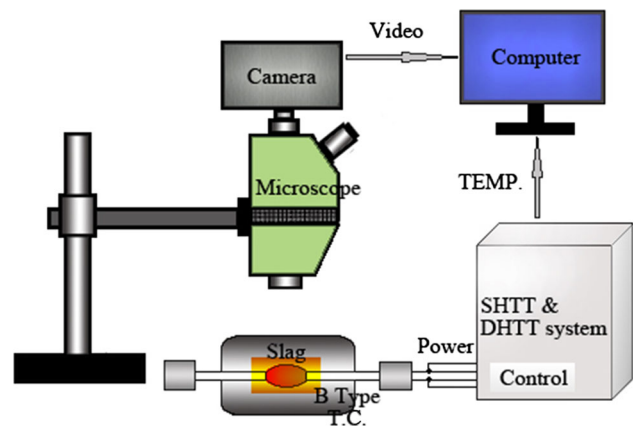


Fig. 1—Schematic drawing of double hot thermocouple technology.

Table I. The Major Chemical Compositions of Mold Fluxes (in Mass Pct)

Sample	R	CaO	SiO_2	Al_2O_3	B_2O_3	Li_2O	F
1	1.25	43.06	34.44	4	0	1	8
2	1.15	41.72	36.28	4	6	2	0
3	1.2	42.55	35.45	4	6	2	0
4	1.25	43.33	34.67	4	6	2	0
5	1.15	40.65	35.35	4	6	4	0
6	1.15	39.58	34.42	4	6	6	0

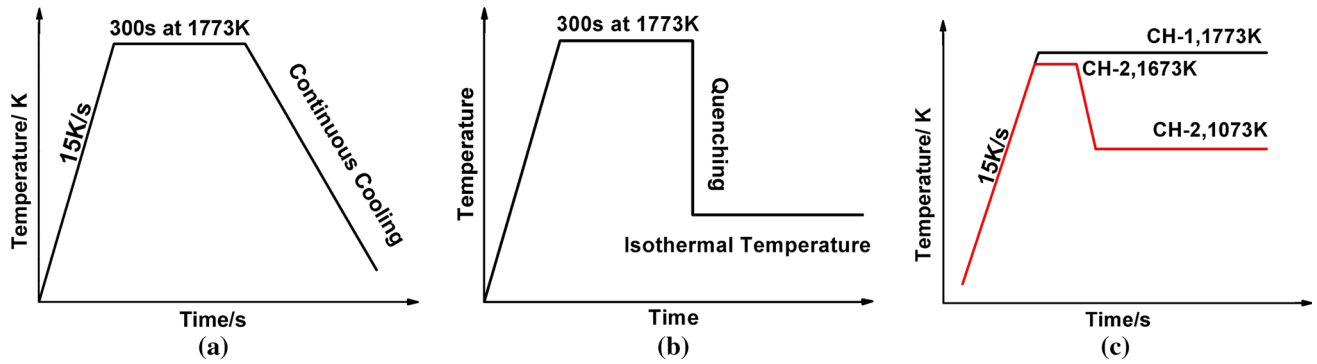


Fig. 2—Thermal profiles for (a) CCT test, (b) TTT test, and (c) DHTT test.

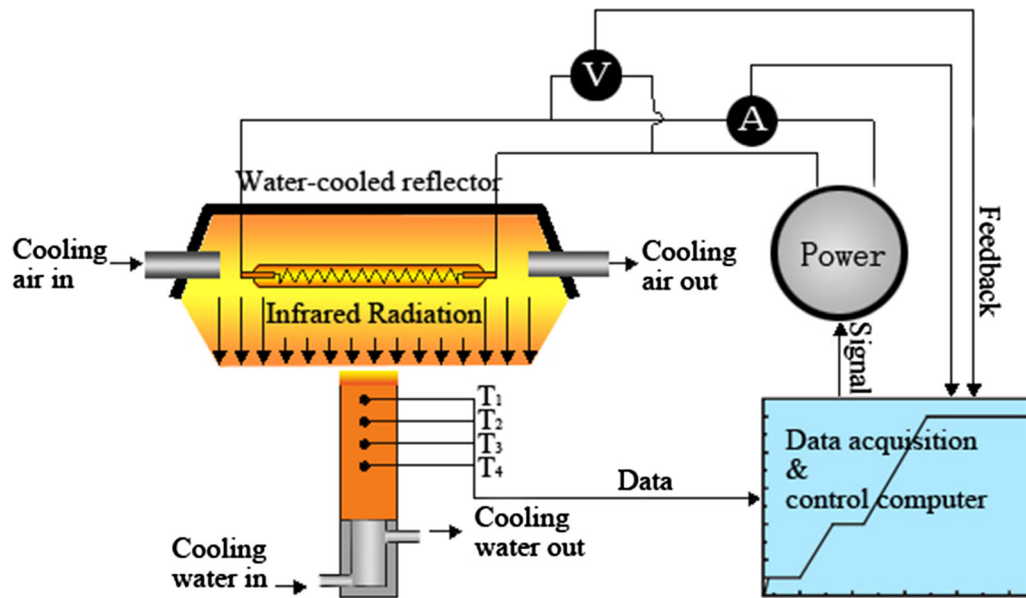


Fig. 3—Schematic figure of the infrared emitter.

illustration of IET is shown in Figure 3, It includes the following units: a power controller, an infrared radiant heater with the capability of emitting 2.0 MW/m^2 heat flux at 380 voltages, a data acquisition, and control system.^[13,15] The wavelength of IET was in the range from 0.7 to 8 micron with a peak of 1.2 micron, which was similar to heat wavelength emitted from the solidifying shell during the continuous casting process as indicated in previous studies.^[13,16]

In order to avoid the internal thermal stresses and cracks in the mold flux disks caused by rapid heating, the emitting energy was increased linearly at a constant heating rate of $1 \text{ KW/m}^2\text{s}$ with three holding stages (500, 800, 1400 KW/m^2) that is shown in Figure 4 during the experimental process.

As shown in Figure 3, four thermocouples are embedded in the positions that are 2, 5, 10, and 18 mm under the irradiated surface, and the temperature is recorded as T1, T2, T3, and T4, respectively.

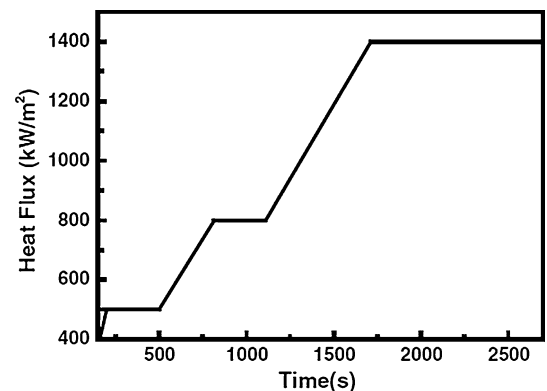


Fig. 4—Heating profile for IET experiments.

Thus the responding heat transfer rate can be calculated using this temperature gradient as previous studies.^[13,17,18]

D. The Phase Analysis

The phase of slag disks after the heat transfer test and the morphology of crystalline phases in the disks were further observed through Scanning Electron Microscope (Japanese Electronics Company JSM-6360LV) with an acceleration voltage of 20 kW and $\times 1000$ magnification. The crystalline phases developed during the heat transfer tests and TTT tests were analyzed by Energy Dispersive Spectrometer (America EDAX Corporation EDX-GENESIS 60S) and X-ray Diffractometer (Rigaku Corporation RIGAKU-TTR III) with Cu K α (0.154184 nm). The XRD data were collected in a range of $2\theta = 10$ -80 deg with a step size of 10 deg/minute. The samples for SEM and EDS analysis were prepared through polishing the disks after the heat transfer test; then those disks were crushed into powders for XRD test. Besides, considering the sample from the TTT tests were too small, which is not enough for the XRD test, the crystalline phases precipitated at the lower- and higher-temperature zones were investigated through preparing the samples at the temperatures of 1273 K and 1473 K (1000 °C and 1200 °C), separately in an electric furnace, and then crushed into powders for XRD test.

III. RESULTS AND DISCUSSION

A. Melting Behavior

It is well known that the mold flux has no fixed melting point, as it is a multi-component mixture. The melting temperature as an important physicochemical property of mold flux was studied using the single thermocouple technique (CH-1) according to the thermal profile as shown in Figure 2(a). The melting behavior of Sample 1 was chosen as a representative one and shown in Figure 5, where the initial melting temperature was suggested as 1289 K (1016 °C) and the complete melting temperature was 1486 K (1213 °C) as indicated by the deviation of the responding heating curves.

The melting behavior of all mold fluxes were summarized in Figure 6; it could be found that the melting temperature range was improved from [(1306 K to 1500 K (1033 °C to 1227 °C))] to [1356 K to 1529 K

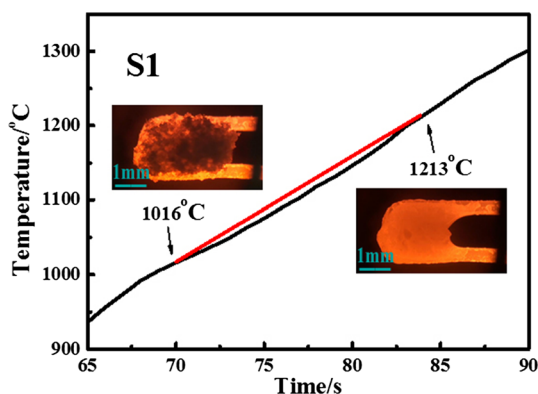


Fig. 5—Melting process of Sample 1.

(1083 °C to 1256 °C)] and [(1360 K to 1550 K (1087 °C to 1277 °C))] for the Samples 2, 3, and 4, when the basicity increases from 1.15 to 1.2 and 1.25, respectively, which suggested that the basicity tends to improve the melting temperature range of mold fluxes. The above issue could be explained as a fact that the high melting point compounds such as Ca₂SiO₄ (melting point 2130 °C) would be easily formed with the addition of CaO,^[5] which would tend to increase the melting temperature range of the resulting mold fluxes.

However, it showed the opposite tendency for the Li₂O series samples. When the Li₂O increases from 2 to 4 and 6 pct, the melting temperature range for Sample 2, 5, and 6 was reduced from [1306 K to 1500 K (1033 °C to 1227 °C)] to [(1299 K to 1488 K (1026 °C to 1215 °C))] and [1288 K to 1475 K (1015 °C to 1202 °C)], respectively. The above phenomena is due to the fact that as an effective fluxing agent, Li₂O itself belongs to the low melting point compound which does contribute to the reduction of the system melting temperature. Also the electrostatic potential of Li⁺ (1.47 Å) is very close to that of SiO₄⁴⁻ (1.44 Å),^[12] which would hinder the tendency of other cation such as Ca²⁺ to combine with SiO₄⁴⁻ to form high melting point compound *e.g.*, Ca₂SiO₄ (melting point 2130 °C).

B. Crystallization Behavior

As one of the main parameters to characterize the mold flux crystallization behavior, the continuous cooling tests (CCT) have been conducted, and Figure 7(a) through (f) show the CCT diagrams of above mold flux samples, also the crystallization temperatures under different cooling rate are listed in Table II. It could be observed that the crystallization temperature decreases with the increase of continuous cooling rate. The reason may be due to the increase of molten slag viscosity with the increase of cooling rate.^[19] As viscosity increases very quickly, it requires a stronger driving force to initiate the nucleation in the mold flux, which means a larger under-cooling is required. Therefore, the crystallization temperature decreases with the increase of continuous cooling rate.

It was found that all the critical cooling rate of slags including F-containing Sample 1 is over 30 K/second, which is beyond the upper limit of the testing equipment

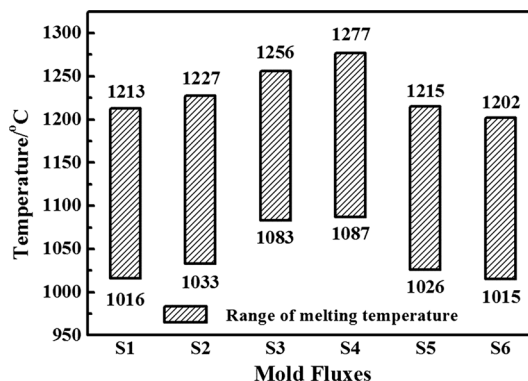


Fig. 6—The melting temperature range for all sample slags.

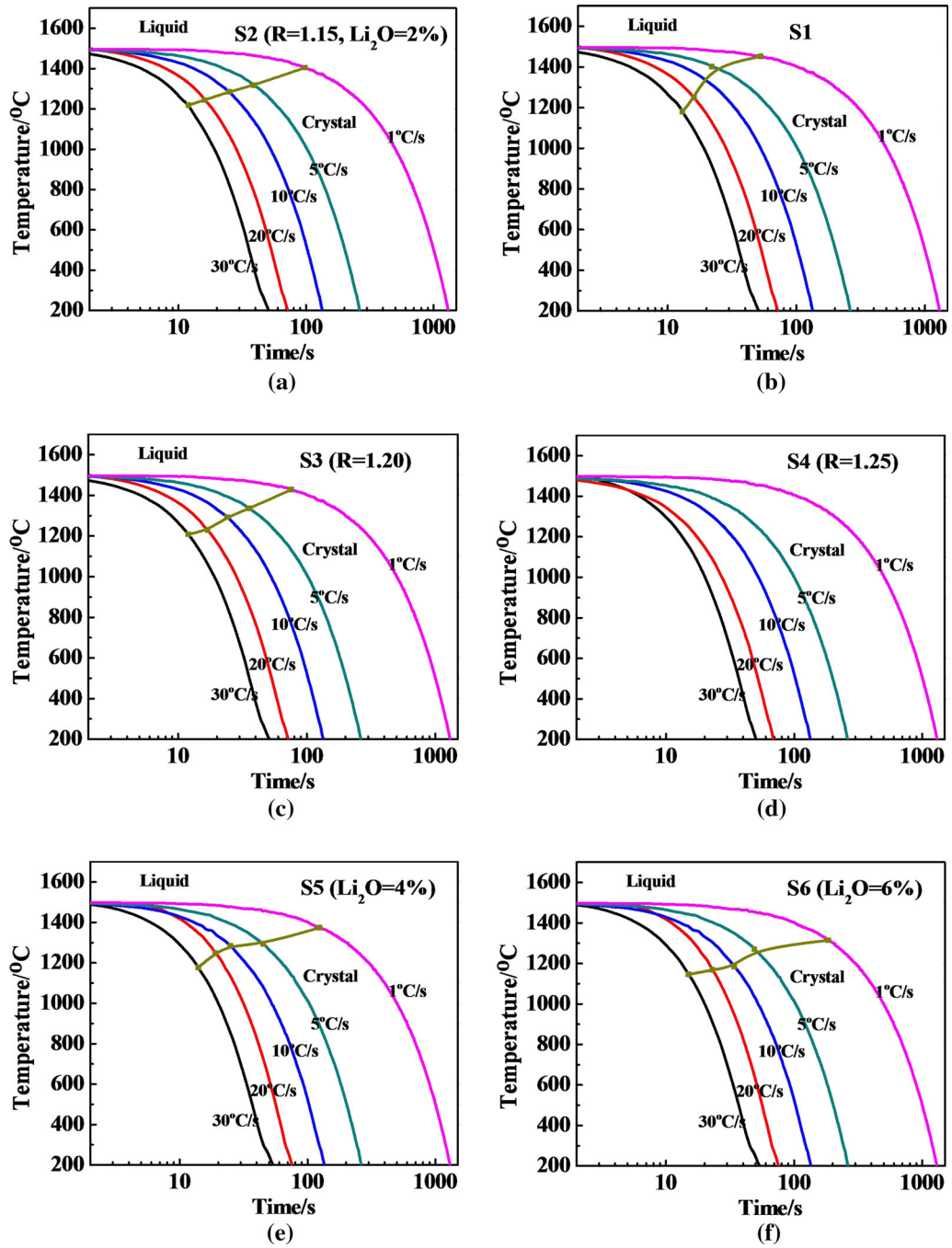


Fig. 7—CCT diagrams of (a) Sample 1, (b) Sample 2, (c) Sample 3, (d) Sample 4, (e) Sample 5, and (f) Sample 6.

Table II. Crystallization Temperature at Different Cooling Rate

Cooling Rate	Samples					
	1	2	3	4	5	6
1 K (°C)/s	1452	1405	1428	1500	1373	1315
5 K (°C)/s	1402	1317	1336	1500	1294	1270
10 K (°C)/s	1324	1285	1293	1500	1284	1185
20 K (°C)/s	1249	1243	1229	1500	1247	1168
30 K (°C)/s	1180	1219	1208	1500	1177	1146

used in this study. Therefore, no exact figure of critical cooling rate was given for above samples. It suggests that the mold fluxes used for casting medium carbon steels do own a strong crystallization tendency.

For Samples 2, 3, and 4 with varied basicity, the crystallization temperature (T_c) increases from 1678 K to 1701 K (1405 °C to 1428 °C) and 1773 K (1500 °C), with the increase of basicity, when the cooling rate was fixed at 1 K/second. It indicates that basicity tends to enhance mold flux crystallization significantly. The main reason is that CaO belongs to basic oxide, which would offer Non-bridged Oxygen to break the silicate structure;^[20,21] therefore, the crystallization of mold flux would get enhanced as the movement of particles becomes easier due to the decrease of diffusion resistance, which is beneficial for the nucleation and aggregation of crystals.^[22] However, for the Samples 2, 5, and 6, the crystallization temperature decreases with the increase of Li_2O , where it decreases from 1678 K to 1646 K (1405 °C to 1373 °C) and 1588 K (1315 °C), respectively, when cooling rate was fixed at 1 K/s. The reduction of the crystallization temperature could be attributed to the fact that the electrostatic potential of Li^+ (1.47 Å) is very close to that of SiO_4^{4-} (1.44 Å), which would hinder the other cations to combine with SiO_4^{4-} to form crystals.^[12] As a result, the

formation of high melting point compound *e.g.*, Ca_2SiO_4 (melting point 2130 °C) is inhibited and the crystallization temperature is reduced with the increase of Li_2O content.

In order to study the structure of the mold flux film infiltrated between the mold hot surface and initial solidified shell, the crystallization behavior of mold flux subjected to the temperature gradient as shown in Figure 2(c) was investigated through DHTT test, and the relative thickness of each layer was calculated from the recorded real-time image. The DHTT images corresponding to above samples are shown in Figure 8, where it was observed that the distribution of each layer is very apparent. The left side of the sample next to the high-temperature side (CH1) is the liquid layer, while the right is the crystalline layer close to the lower-temperature side (CH2). For the benchmark Sample 1, it is found that the thickness of the crystalline layer is 94.55 pct, while the liquid layer is 5.45 pct, which suggests that the F-containing mold flux for casting medium carbon steels does own strong crystallization property and high crystallization ratio.

For the Samples 2, 3, and 4 with varied basicity, the thickness of the crystalline layer was observed to increase obviously from 88.89 to 94.55 and 96.30 pct

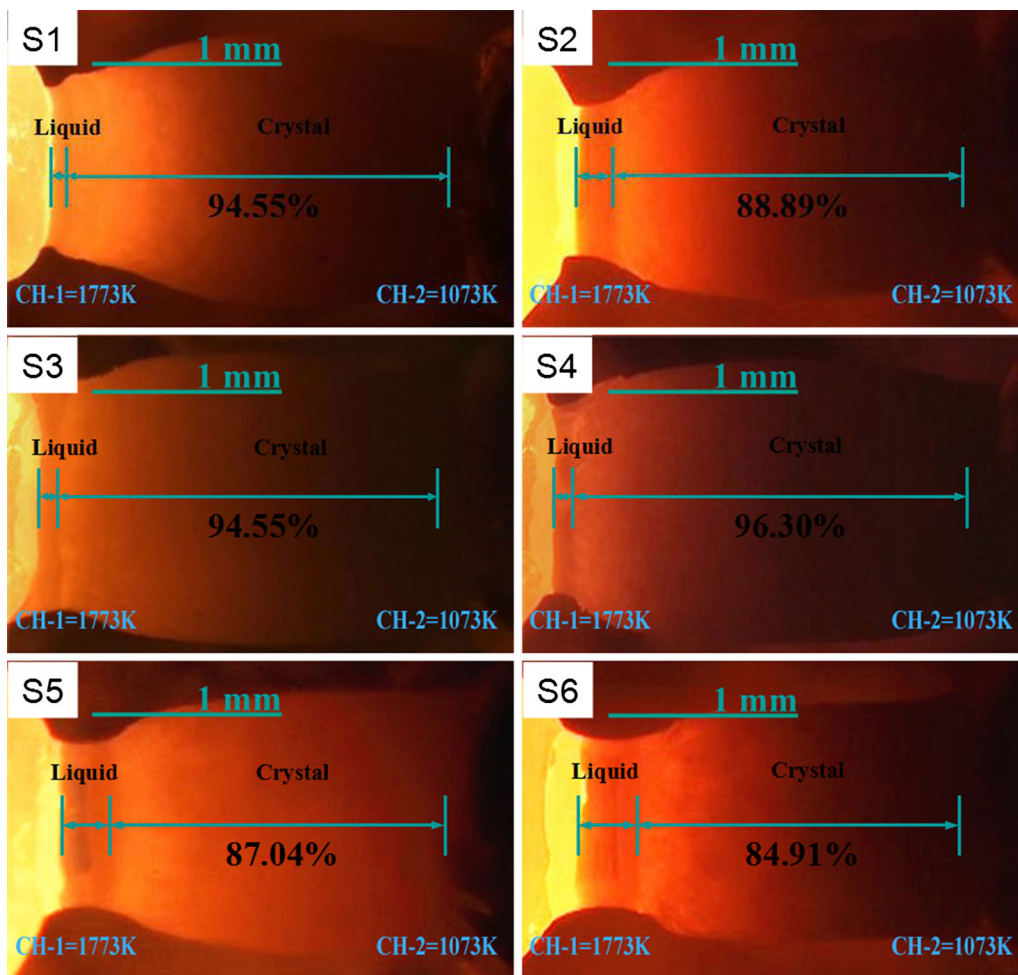


Fig. 8—Steady-state DHTT images for Samples 1 to 6.

when the basicity is improved from 1.15 to 1.20 and 1.25, respectively. It indicates that the basicity has the significant capability to enhance crystallization of the mold flux, which agrees with the results of the above CCT tests. However, for the Samples 2, 5, and 6, when the Li_2O content was increased from 2 to 4 and 6 pct, the thickness of the crystalline layer decreases from 88.89 to 87.04 and 84.91 pct, respectively, and it suggested that high content of Li_2O does reduce the crystallization temperature as indicated in above CCT tests. Therefore, the liquid layer was increased with the addition of Li_2O in the mold flux.

In order to further study the effects of Li_2O on the mold flux crystallization behavior, the TTT test of Samples 2, 5, and 6 were conducted. Figure 9 shows TTT curves of Samples 2, 5, and 6, respectively; it can be seen that the incubation time for all the fluxes is very short when they are isothermally crystallized at 1473 K (1200 °C). Therefore, it is clear that all the fluxes used in this study have a great crystallization tendency as suggested from both TTT and CCT tests. For Sample 2, the TTT diagram has two distinct noses, which are indicated as Ca_2SiO_4 and $\text{Ca}_{11}\text{Si}_4\text{B}_2\text{O}_{22}$ in high-temperature zone and $\text{Ca}_{11}\text{Si}_4\text{B}_2\text{O}_{22}$ in low-temperature zone that will be described later in Section III-D. While the shape of the curves of Samples 5 and 6 are similar to each other, and these two samples crystallized very fast with an incubation time of almost 0 second when the crystallization temperature is lower than 1473 K (1200 °C).

The 95 pct crystallization TTT curves of Samples 2, 5, and 6 are combined in Figure 10, and it shows that in the high-temperature zone above 1473 K (1200 °C), the incubation time becomes much longer with the increase of Li_2O content, where the TTT curve of a higher Li_2O content shifts toward the right side obviously, indicating that Li_2O suppresses the high-temperature crystallization process within the experimental range. However, in the low-temperature zone below 1273 K (1000 °C), the TTT curve of higher Li_2O content shifts toward the left side, when Li_2O content was in the range of 2 to 6 pct, indicating that Li_2O strengthens the low-temperature crystallization process. The phenomenon is consistent with the study of Lu^[1] and will be verified later in Section III-D.

C. Heat Transfer Behavior

The glass disks of each sample that were prepared according to Section II-A were placed on top of the copper mold and subjected to the thermal heating individually as shown in Figure 3. In order to well understand the heat transfer behavior of each mold flux, the responding heat flux for benchmark Sample 1 from the time period of 500 to 2400 seconds as well as its real-time disk images are selected and presented in Figure 11.

There are six stages appearing in the responding heat flux history. Stage I is a period in which the heat flux increases linearly with the increase of thermal radiation. Stage II is the period of a constant state when the incident heating energy keeps constant.^[22] From the screenshots, it is clearly shown that the reddish mold flux disk (at 500 seconds) is in a mixture state of major glass and slight crystal across the surface in stage I; and this state does not seem to change as shown in the disk at 1000 seconds, which explained the constant heat flux at stage II. In stage III, it was observed that the milky crystallization was precipitated from the top of the disk and developed gradually toward the bottom seen from 1100 to 1400 seconds with the increase of thermal heating. In stage IV, the melting of the slag top surface is clearly appearing as shown in the disk photos at 1700 and 1900 seconds, where the top surface is deformed and riffling with the further increase of incident energy.

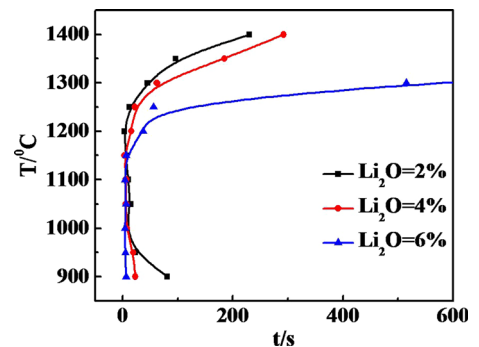


Fig. 10—Comparison of 95 pct crystallization TTT diagrams of mold fluxes with different Li_2O contents.

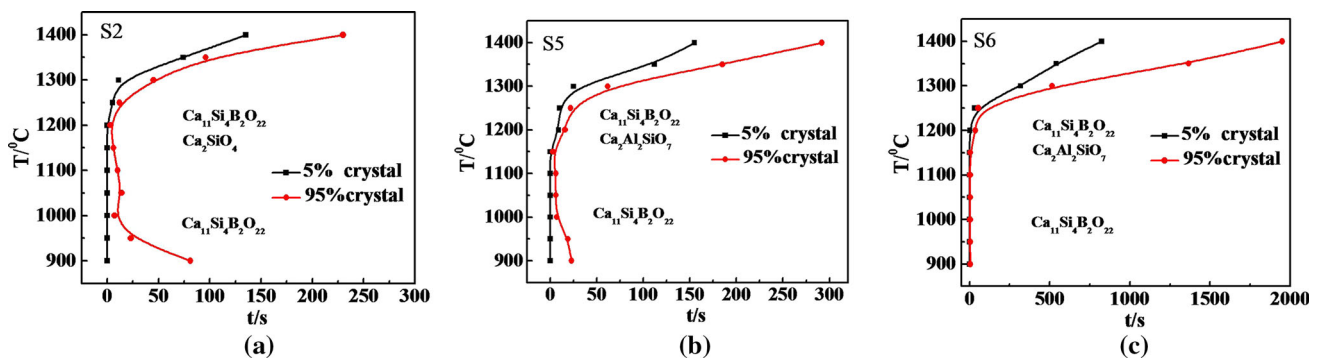


Fig. 9—TTT diagrams of mold fluxes with different Li_2O contents: (a) Sample 2=2 pct, (b) Sample 5=4 pct, and (c) Sample 6=6 pct.

Stage V is an attenuation stage where the heat flux continues to reduce under the constant thermal radiation as a balance of further crystallization and melting. Stage VI is the period of relative steady state when the dynamic phase transformation is completed and the heat flux keeps constant.

In order to further investigate the influence of crystallization and melting on the heat transfer behavior, the heat flux from 1200 to 1750 seconds was chosen and shown in Figure 12. With the development of crystallization, the responding heat flux began to reduce at 1257 seconds, when the heating energy is linearly increased. The main reason for this reduction is due to the reflection and scattering of the radiation at the positions of the crystal surface, grain boundary, as well as defects with the further development of mold flux crystallization.^[13] Contrary to crystallization phase transformation, the liquid phase was occurred at 1549 seconds on the top surface of mold flux disk, and the responding heat flux was observed to increase. This is attributed to the fact that the melting of the mold flux tends to enhance the overall heat transfer rate in the continuous casting.

The heat flux curves of R series and the benchmark flux Sample 1 were plotted in Figure 13. It shows that

the responding steady-state heat flux decreases as R increases, and the overall heat transfer behavior of Sample 3 and Sample 4 is close to benchmark flux Sample 1. Above results suggested that the overall heat transfer rate reduces with the increase of basicity, as the mold flux with improved crystallization capability would block more incident radiation and introduce a larger interfacial thermal resistance that would result in a lower heat transfer rate as suggested in the previous studies.^[19,22]

D. The Results of SEM/EDS and XRD

In order to study the variation of the precipitated phase and the crystal morphology, scanning electron microscopy (SEM), energy dispersive spectroscopy (EDS), and X-ray diffraction (XRD) were applied for the analysis of above disk samples after IET tests.

The SEM images and the typical EDS results were shown in Figures 14(a) and (b), the position of each sample from the upper, middle, to bottom part is marked as layer A, layer B, and layer C from the left to the right side, respectively. For all disk samples, it is found that the size of crystals distributed from upper to bottom in all disk samples become small while the number of crystals is increased due to the increase of the cooling rate. It is obvious that the major beautiful sphere-type cuspidine (I: $\text{Ca}_4\text{Si}_2\text{O}_7\text{F}_2$) crystals were formed in the Sample 1, and a small part of gehlenite (II: $\text{Ca}_2\text{Al}_2\text{SiO}_7$) formed in the layer b, which is consistent with the XRD results as shown in Figure 15(a). It well explains why cuspidine is a very important crystalline phase for the mold flux crystallization, as this typical morphology is very beneficial for the control of the mold heat flux transfer and lubrication.

For Samples 2, 3, and 4 with varied basicity, the main crystal phases existing in the high-temperature zone are the pellet or blocky dicalcium silicate (IV: Ca_2SiO_4) and strip-like calcium borate silicate (III: $\text{Ca}_{11}\text{Si}_4\text{B}_2\text{O}_{22}$) that crystallized from the liquid phase, which was also identified by XRD results as shown in Figure 15(b). It is clear that the crystallization ratio

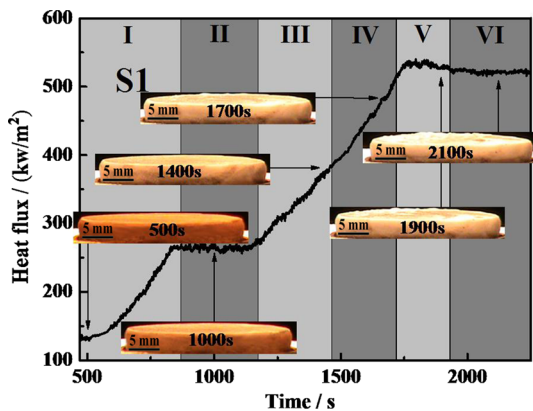


Fig. 11—The responding heat flux of Sample 1 vs time.

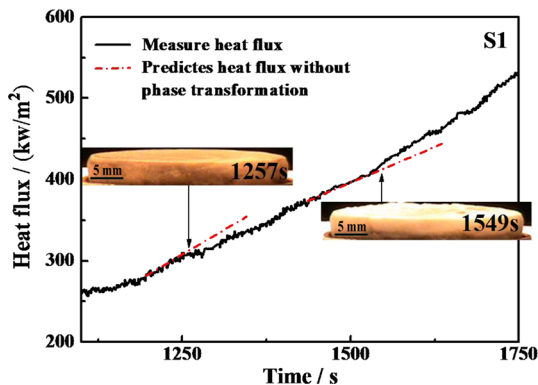


Fig. 12—Slag disks of Sample 1 at the crystallization and melting point.

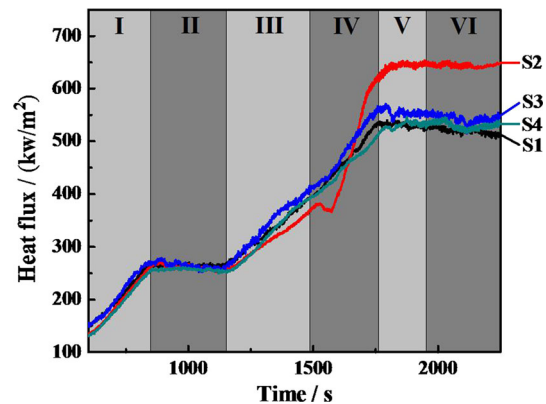
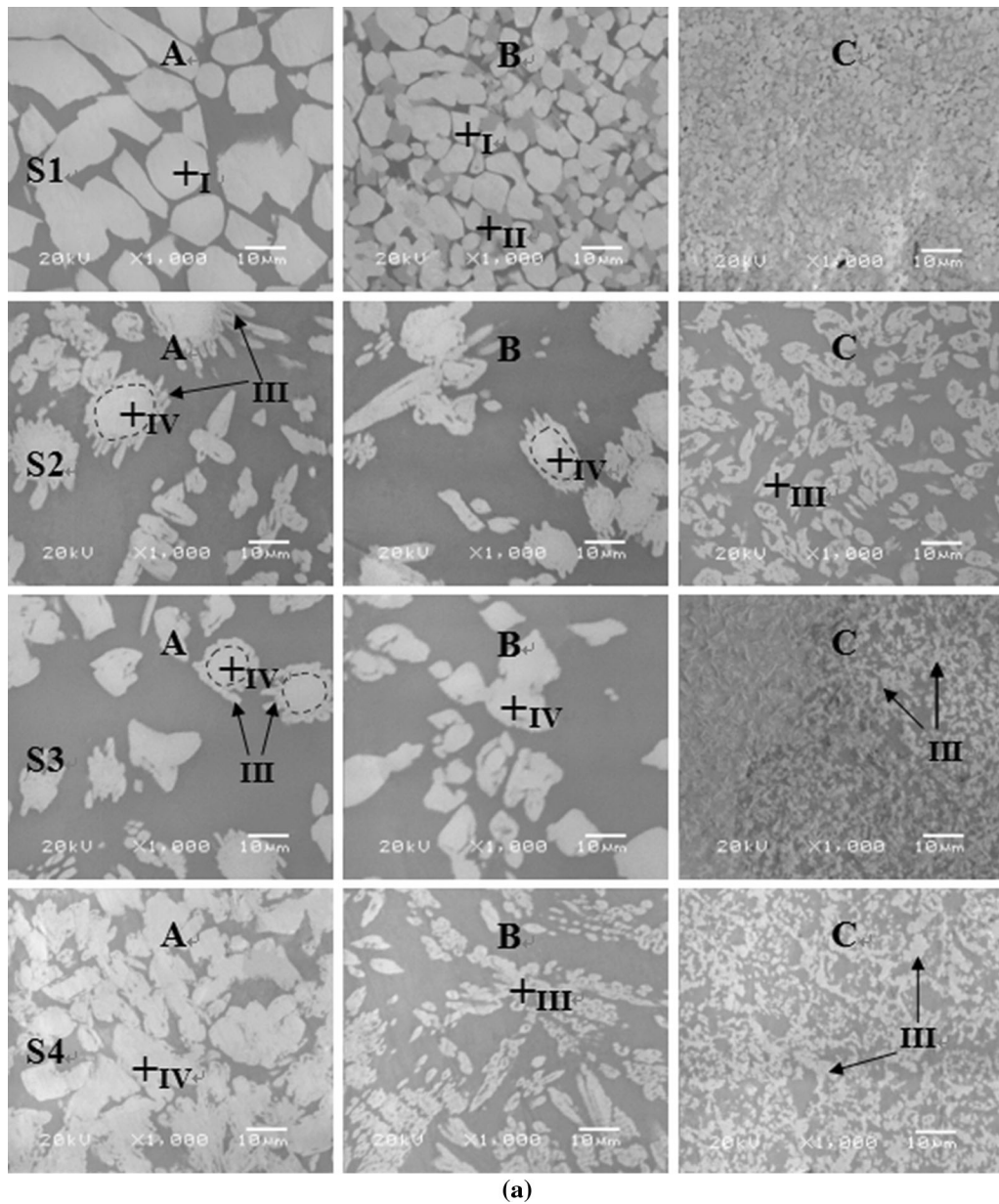


Fig. 13—Effect of basicity on the heat fluxes for Sample 2(R=1.15), Sample 3(R=1.20), and Sample 4(R=1.25).



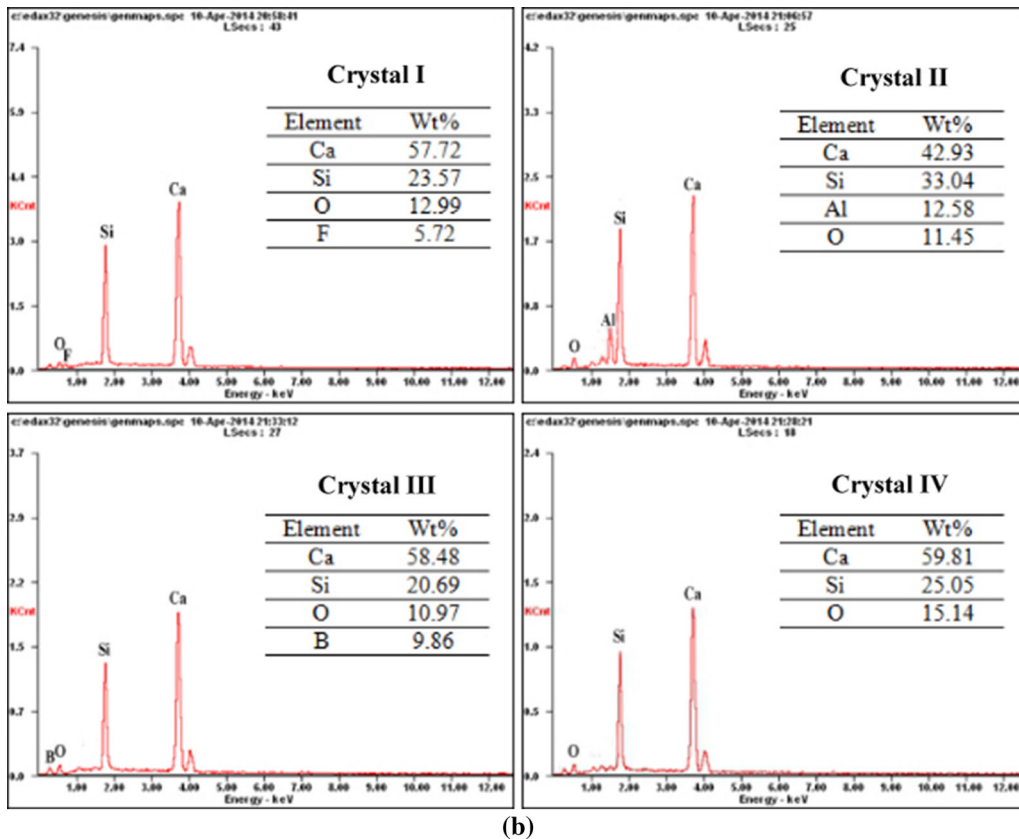
(a)

Fig. 14—(a) The SEM images and (b) the corresponding EDS of crystals in the disk samples after IET tests.

was improved with the increase of basicity, which is consistent with above CCT and DHTT results. Comparing Sample 1 with Sample 4, these two samples show very similar heat transfer and crystallization behavior; however, the difference is that the Sample 4 did not appear in the sphere-type crystalline morphology that is well distributed in Sample 1. Also, the crystal phase of dicalcium silicate was observed from the XRD results as shown in Figure 15(b). The amount of dicalcium silicate seems to increase with the improvement of basicity, as the values of the highest characteristic peak of dicalcium silicate in Figure 15(b) are 75, 84, and 91 for Samples 2, 3, and 4,

respectively. So, the result of XRD suggests that basicity does enhance the precipitation of high melting point phase of dicalcium silicate, especially when there is no borate silicate phase formed in the high-temperature zone in Sample 4 (in Figure 14(a) S4 sample). It could also be observed that borate silicate phase is also formed from the crystallization of glassy phase as shown in the region C in Figure 14(a) for S2, S3, and S4.

Figure 16 shows the XRD results for Samples 2, 5, and 6 used in TTT tests. As shown in Figure 16(a), for Sample 2, a mixture of Ca_2SiO_4 (melting point 2130 °C) and $\text{Ca}_{11}\text{Si}_4\text{B}_2\text{O}_{22}$ (melting point 1440 °C) is observed in



(b)

Fig. 14—continued.

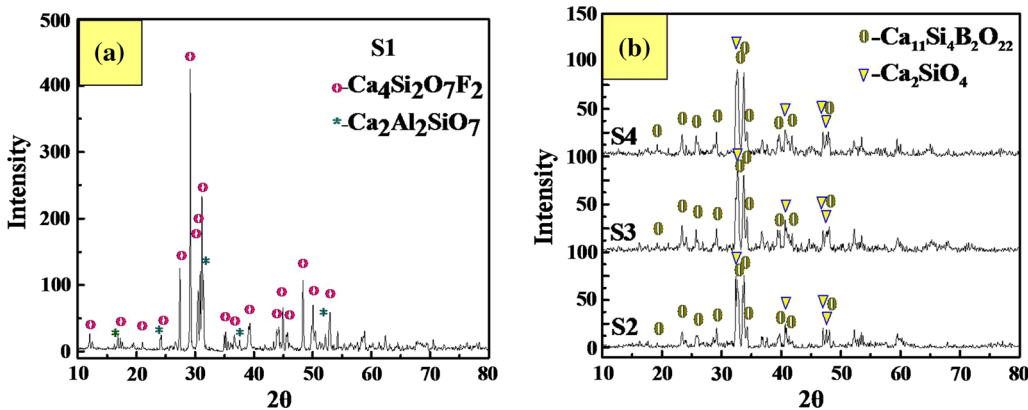


Fig. 15—XRD patterns of the disk samples: (a) Sample 1 with F and (b) samples with varied basicity.

higher-temperature zone, while only $\text{Ca}_{11}\text{Si}_4\text{B}_2\text{O}_{22}$ is precipitated in lower-temperature zone. For Samples 5 and 6, $\text{Ca}_{11}\text{Si}_4\text{B}_2\text{O}_{22}$ together with $\text{Ca}_2\text{Al}_2\text{SiO}_7$ (melting point 1596°C) are formed in high-temperature zone, while only $\text{Ca}_{11}\text{Si}_4\text{B}_2\text{O}_{22}$ precipitated in lower-temperature zone. It indicated that the precipitation of high

melting point phase of dicalcium silicate gets suppressed with the addition of Li_2O content. In addition the peak intensity of $\text{Ca}_{11}\text{Si}_4\text{B}_2\text{O}_{22}$ is significantly increased, indicating that Li_2O tends to accelerate the formation of lower-temperature phase $\text{Ca}_{11}\text{Si}_4\text{B}_2\text{O}_{22}$, which is consistent with the TTT results.

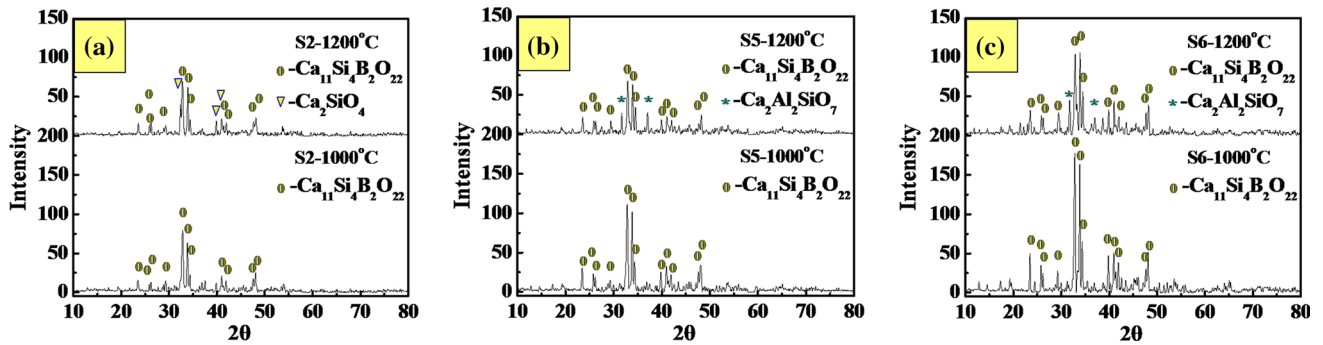


Fig. 16—XRD patterns of mold fluxes with different Li_2O contents: (a) Sample 2 = 2 pct, (b) Sample 5 = 4 pct, and (c) Sample 6 = 6 pct.

IV. CONCLUSIONS

The effects of basicity and Li_2O on the melting, crystallization, and heat transfer behaviors of fluoride-free mold fluxes for casting medium carbon steels were studied and compared with a typical industrial F-containing mold flux. The major conclusions are summarized as follows:

1. The melting tests show that the melting temperature of the designed F-free mold flux was increased with the addition of basicity due to the fact that the addition of CaO could easily form high melting point compound Ca_2SiO_4 ; while the addition of Li_2O shows the opposite effect as Li_2O itself belongs to the lower melting point fluxing agent and could hinder the formation of high melting point compound.
2. The CCT and DHTT tests indicated that basicity would improve the crystallization temperature and promote the crystallization of mold flux. While the CCT and DHTT tests consistently indicated that Li_2O tends to lower the crystallization temperature, as it would hinder other cations to combine with SiO_4^{4-} to form high melting point crystals. The TTT tests suggested that Li_2O would tend to inhibit the crystallization of F-free mold fluxes in high-temperature region and greatly accelerate the crystallization behavior of F-free mold fluxes in low-temperature region.
3. The IET tests indicated that the heat transfer of mold flux was restrained when the basicity of mold flux was improved, as it tends to promote the mold flux crystallization.
4. The results of SEM/EDS and XRD consistently demonstrated that the main crystal phase in the F-free mold fluxes is calcium borate silicate ($\text{Ca}_{11}\text{Si}_4\text{B}_2\text{O}_{22}$), which shows the potential to replace cuspidine in the designed F-free mold flux system.

ACKNOWLEDGMENTS

The financial support from NSFC (51274244, 51322405), the Natural Science Foundation of Hunan

Province China (Grant No. S2015J504I), and the grant from the project of Innovation-driven plan in Central South University are greatly acknowledged.

REFERENCES

1. B. Lu, W. Wang, K. Chen, and B. Jiang: *Metall. Mater. Trans. B*, 2014, vol. 45B, pp. 1496–1509.
2. S.Y. Choi, D.H. Lee, D.W. Shin, S.Y. Choi, J.W. Cho, and J.M. Park: *J. Non-Cryst. Solids*, 2004, vols. 345–346, pp. 157–60.
3. H. Nakada and K. Nagata: *ISIJ Int.*, 2006, vol. 46 (3), pp. 441–49.
4. L. Zhou, W. Wang, J. Wei, and K. Zhou: *ISIJ*, 2015, vol. 55 (4), pp. 821–829.
5. Z. Zhang, G. Wen, and Y. Zhang: *Int. J. Miner.*, 2011, vol. 18 (2), pp. 150–58.
6. A.I. Zaitsev, A.V. Leites, A.D. Litvina, and B.M. Mogutnov: *Steel Res.*, 1994, vol. 65, p. 368.
7. L. Zhou, W. Wang, B. Lu, G. Wen, and J. Yang: *Metal Mater. Int.*, 2015, vol. 21 (1), pp. 126–133.
8. X. Qi, G.H. Wen, and P. Tang: *J. Non-Cryst. Solids*, 2008, vol. 354, pp. 5444–52.
9. Q. Wang, Y. Lu, S. He, K.C. Mills, and S. Li: *Ironmak. Steelmak.*, 2011, vol. 38 (4), pp. 297–301.
10. J. Wei, W. Wang, L. Zhou, D. Huang, H. Zhao, and F. Ma: *Metall. Mater. Trans. B*, 2014, vol. 45B, pp. 643–52.
11. L.G. Zhu, G.Z. Tang, A.Z. Wang, and S.T. Jin: *Iron Steel*, 2000, vol. 35 (11), pp. 23–26.
12. H. Liu, G.H. Wen, and P. Tang: *ISIJ Int.*, 2009, vol. 49 (6), pp. 843–50.
13. K. Gu, W. Wang, L. Zhou, F. Ma, and D. Huang: *Metall. Mater. Trans. B*, 2012, vol. 43B, pp. 937–45.
14. Y. Kashiwaya, T. Nakauchi, K.S. Pham, S. Akiyama, and K. Ishii: *ISIJ Int.*, 2007, vol. 47 (1), pp. 44–52.
15. W. Wang and A.W. Cramb: *ISIJ Int.*, 2005, vol. 45 (12), pp. 1864–70.
16. J. Cho, H. Shibata, T. Emi, and M. Suzuki: *ISIJ Int.*, 1998, vol. 38 (5), pp. 440–46.
17. W. Wang, K. Gu, and L. Zhou: *ISIJ Int.*, 2011, vol. 51 (11), pp. 1838–45.
18. K. Gu, W. Wang, J. Wei, H. Matsuura, F. Tsukihashi, I. Sohn, and D. Min: *Metall. Mater. Trans. B*, 2012, vol. 43B, pp. 1393–04.
19. L. Zhou, W. Wang, F. Ma, J. Li, J. Wei, H. Matsuura, and F. Tsukihashi: *Metall. Mater. Trans. B*, 2012, vol. 43B, pp. 354–62.
20. K.C. Mills: *ISIJ Int.*, 1993, vol. 33 (1), pp. 148–55.
21. M. Persson, M. Gornrup, and S. Seetharaman: *ISIJ Int.*, 2007, vol. 47 (10), pp. 1533–40.
22. B. Lu, W. Wang, J. Li, H. Zhao, and D. Huang: *Metall. Mater. Trans. B*, 2013, vol. 44B, pp. 365–77.